Electrodeposition of iron core-shell nanoparticles on a H-terminated Si(100) surface

L. Y. Zhao, K. R. Eldridge, K. Sukhija, H. Jalili, N. F. Heinig, and K. T. Leung[a)]
Departments of Chemistry, University of Waterloo, Waterloo, Ontario N2L 3G1, Canada

(Received 6 September 2005; accepted 15 December 2005; published online 19 January 2006)

Iron core-shell nanoparticles with different morphologies were obtained on a H-terminated Si(100) surface for the first time by electrodeposition at different $FeCl_3$ concentrations. At 10 mM, near-monosized and uniformly distributed oval-shaped nanorod Fe particles (130 nm length $\times$25 nm diameter), with a mixed FeOOH and FeO shell, have been obtained. At 0.1 mM, spherical Fe nanoparticles (6–40 nm diameter) with a broader size distribution and a mixed Fe_2O_3 and FeO shell were observed. The morphologies and compositions of these two types of Fe core-shell nanoparticles could be easily manipulated to provide magnetic properties of potential industrial interest. © *2006 American Institute of Physics*. [DOI: 10.1063/1.2165180]

Magnetic nanoparticles, particularly iron with its low cost advantage and biological compatibility, have attracted significant recent attention due to their potential applications in magnetic recording media and data storage[1] and targeted drug delivery.[2] Several synthesis techniques for these iron nanoparticles have been reported. Gangopadhyay *et al.* obtained near-spherical Fe nanoparticles by thermal evaporation and condensation of bulk metal in an inert atmosphere.[3] Particle size ranging from 6 to 35 nm could be obtained at different argon pressures, and the α-Fe core was found to be surrounded by Fe oxides. Using a biased scanning tunneling microscopy tip to initiate chemical vapor deposition involving gaseous $Fe(CO)_5$, Li *et al.* and others produced arrays of cylindrical Fe nanoparticles with a high aspect ratio (100–120 nm in length and 10 nm diameter) in high precision.[4–6] Jain *et al.* synthesized Fe nanoparticles directly on a Si(100) substrate with and without an Al buffer layer by electron beam deposition from a Fe_2O_3 source.[7] Located between the Fe_2O_3 layer and the Si substrate, the Fe nanoparticles so produced were found to be amorphous with an average grain size of 5 nm. Hosein *et al.* prepared metallic Fe nanoparticles (with an average height of 4–6 nm as determined by atomic force microscopy) by first transferring ferritin on a SiO_2 support, and then followed by removal of the protein shell and reduction of the FeOOH nanoparticles in hydrogen.[8] Among the various methods used to prepare nanoscale metal particles, electrodeposition is a powerful attractive technique because not only is it a simple and inexpensive method but also the particle size, density, and distribution so produced could be easily controlled with high throughput by manipulating the deposition potential, current and/or other parameters. To date, despite a great deal of work involving electroplating of Fe films in the literature,[9] electrodeposition of Fe nanoparticles has not been reported.

In the present work, Fe nanoparticles are prepared by electrochemical deposition on a H-terminated Si(100) surface from an aqueous $FeCl_3$ solution. Unlike electroplating, in which Fe was usually deposited as a film in an acidic solution of ferrous salts, we show that controlled electrodeposition of Fe in the form of discrete metallic nanoparticles with different morphologies can be achieved from a ferric solution. The present result can also be used to develop a simple lithographic method for magnetic nanostructured materials by directed magnetic nanoparticle deposition guided by an external magnetic field.

All the electrodeposition experiments were performed in a three-electrode cell with a potentio/galvanostat electrochemical workstation (CH Instruments 660A) using a similar procedure discussed in our recent work.[10] The working electrodes were single-side-polished rectangular (15×2.5 mm^2) Si(100) chips (0.4-mm-thick, *p* type with a resistivity of 1.0–1.5 mΩ cm), which have been H-terminated by a standard procedure described elsewhere.[11] A standard Ag/AgCl reference electrode was used while a platinum wire was used as the counter electrode in all the electrodeposition experiments. In a deoxygenated aqueous solution of 0.1–20 mM $FeCl_3$ and 0.1 M $NaClO_4$ (serving as the electrolyte), Fe nanoparticles were deposited on the H-terminated Si substrate potentiostatically by amperometry at a constant potential of −0.8 V (relative to the Ag/AgCl reference electrode). The deposition time was controlled by fixing the amount of charge transfer, typically at 1.2×10^{-4} C for a 10 mM $FeCl_3$ solution and 5×10^{-3} C for a 0.1 mM $FeCl_3$ solution. After the deposition, the Si substrate was removed from the cell, thoroughly rinsed with Millipore water (18.2 MΩ cm resistivity), and dried in N_2, before further analysis.

The surface morphology of the Fe nanodeposits was characterized by a LEO 1530 field-emission scanning electron microscope (SEM) and a Digital Instruments Nanoscope IV atomic force microscope (AFM), while the corresponding chemical composition was analyzed as a function of depth (depth profiling) by interleaving x-ray photoelectron spectroscopy (XPS) analysis and argon ion sputtering. The XPS depth-profiling experiment was conducted in a Thermo-VG Scientific ESCALab 250 microprobe equipped with a monochromatic Al $K\alpha$ x-ray source (1486.6 eV), operated with a typical energy resolution of 0.4–0.5 eV full width at half maximum. Argon sputtering was performed over a rastered area of 3×3 mm^2 of the sample at an ion beam energy of 3 keV and sample current density of 102 nA mm^{-2}. The corresponding sputtering rate for the Fe nanodeposits was estimated to be 0.9 nm min^{-1}. CasaXPS software was used to analyze the XPS data and background subtraction was done by using the Shirley method.

[a)]Author to whom correspondence should be addressed; electronic mail: tong@uwaterloo.ca

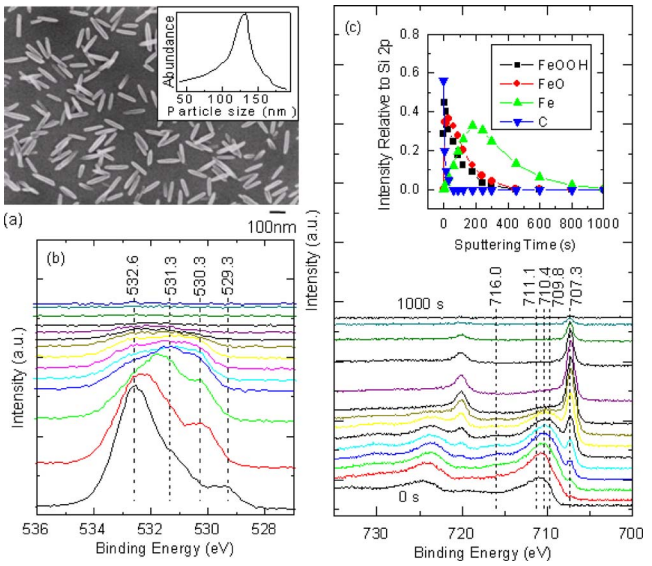

FIG. 1. (Color online) (a) SEM micrograph of oval-shaped nanorod Fe particles obtained by electrodeposition from a solution of 10 mM $FeCl_3$ and 0.1 M $NaClO_4$. The inset shows the relative abundance of the nanorods as a function of their lengths. XPS spectra of (b) O 1*s* and (c) Fe 2*p* regions of the as-deposited nanoparticles (bottom traces) and upon sequential sputtering for 5, 15, 30, 60, 90, 120, 180, 240, 300, 450, 600, 800, and 1000 s (top traces). The inset shows the change of the peak intensity of C 1*s* feature at 284.8 eV, Fe $2p_{3/2}$ features for metallic Fe at 707.3 eV, FeO at 709.8 eV, and FeOOH at 711.1 eV, all relative to Si 2*p*.

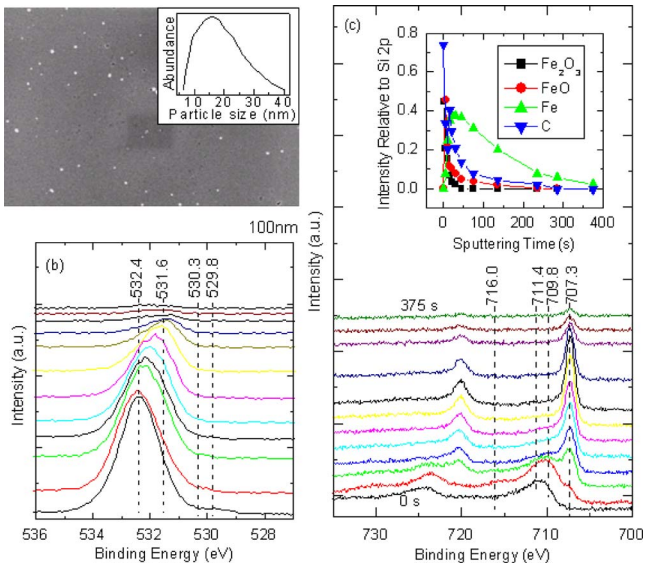

FIG. 2. (Color online) (a) SEM micrograph of spherical Fe nanoparticles obtained by electrodeposition from a solution of 0.1 mM $FeCl_3$ and 0.1 M $NaClO_4$. The inset shows the relative abundance of the nanoparticles as a function of their diameters. XPS spectra of (b) O 1*s* and (c) Fe 2*p* regions of the as-deposited nanoparticles (bottom traces) and upon sequential sputtering for 5, 10, 15, 20, 30, 45, 75, 135, 235, 285, and 375 s (top traces). The inset shows the change of the peak intensity of C 1*s* feature at 284.8 eV, Fe $2p_{3/2}$ features for metallic Fe at 707.3 eV, FeO at 709.8 eV, and Fe_2O_3 at 711.4 eV, all relative to Si 2*p*.

In the present work, we examine the nature of the Fe nanodeposits as a function of $FeCl_3$ concentration. At 0.1 mM $FeCl_3$, only spherical nanoparticles were observed, while at 10 and 20 mM $FeCl_3$, oval-shaped nanorod particles (i.e., "rice" shaped nanoparticles) were obtained. At an intermediate concentration of 1 mM $FeCl_3$, both spherical nanoparticles and oval-shaped nanorods were observed. Figure 1(a) shows a typical SEM micrograph of the electrodeposited Fe nanoparticles obtained at 10 mM $FeCl_3$. Evidently, oval-shaped nanorod particles of 130 nm in length and 25 nm in diameter were uniformly deposited with a narrow size distribution on the H-terminated Si(100) substrate. In the absence of an externally applied magnetic field, there was no apparent long-range ordering in the orientation of these oval-shaped nanorods[12] and the nanorods appeared to be randomly distributed. The chemical composition of the Fe nanorods was examined by XPS, and the corresponding depth profiles of the Fe 2*p* and O 1*s* regions are shown in Figs. 1(c) and 1(b), respectively. The binding energy scale has been calibrated on the C 1*s* feature of residual carbon of the as-deposited sample to the literature value (284.8 eV).[13] The Si $2p_{3/2}$ photopeak (at 99.1 eV) was also found to be in good agreement with the literature,[13] and was subsequently used as a reference for the remaining spectra recorded during the depth-profiling experiment. For the as-deposited oval-shaped nanorod sample [Fig. 1(c)], the Fe $2p_{3/2}$ features at 710.4 and 711.1 eV could be assigned to Fe_3O_4 and FeOOH, respectively.[13] The corresponding O 1*s* features at 529.3, 531.3, and 532.6 eV [Fig. 1(b)] could be attributed to Fe_3O_4, FeOOH, and SiO_2, respectively.[13,14] After 5 s of sputtering, the O 1*s* feature at 529.3 eV [Fig. 1(b)] disappeared, which indicates that the thin Fe_3O_4 surface layer was likely produced in air and not during electrodeposition. Furthermore, two weak emerging features at 707.3 and 716.0 eV were found to correspond to metallic Fe and a Fe^{2+} shake-up process in FeO, respectively. The main Fe $2p_{3/2}$ photopeak for FeO at 709.8 eV was obscured by the broad FeOOH band at 711.1 eV and is not a good signature for FeO. The appearance of the O 1*s* feature at 530.3 eV corresponding to FeO also supports the presence of FeO in the mixed oxide shell. The inset of Fig. 1(c) shows the fitted intensities of various Fe $2p_{3/2}$ features and C 1*s* relative to that of Si 2*p* as a function of the sputtering time (or equivalently depth). Evidently, after the initial removal of air-formed Fe_3O_4 surface layer, the mixed oxide shell was found to be primarily consisted of FeOOH and FeO, with an estimated shell thickness of 25% or ~5 nm of the oval-shaped nanorod structure. This estimate is consistent with the lower limit of 4.2 nm that we obtain from considerations of the attenuation length based on the inelastic mean free path of the electron and the probing depth of the x ray. The considerable amount of the Fe core (75%) in the nanorod structure indicates that the nanorod particle could have substantial ferromagnetic property, and this property will be demonstrated in our future work.[12] It is noteworthy that sputtering of several reference samples of various Fe oxides showed no predominant metallic Fe 2*p* features. The formation of the Fe core in the nanoparticles by reduction of Fe oxides due to sputtering, as observed by Choudhury *et al.*,[14] can therefore be ruled out.

At a lower $FeCl_3$ concentration of 0.1 mM, the nanoparticles obtained by electrodeposition were found to be spherical of 6–40 nm diameter, with a considerably larger (nonhomogeneous) size distribution, as shown in Fig. 2(a). The corresponding XPS spectrum for the as-deposited nanoparticles reveals a strong Fe $2p_{3/2}$ main photopeak at 711.4 eV, which indicates the presence of Fe_2O_3 [Fig. 2(c)].[15] In addition to the strong O 1*s* feature due to SiO_2 from the substrate at 532.4 eV, the weak O 1*s* peak at 529.8 eV could be attributed to Fe_2O_3 [Fig. 2(b)]. Upon sputtering for 5 s, the Fe $2p_{3/2}$ peak for metallic Fe at 707.3 eV and that for FeO at

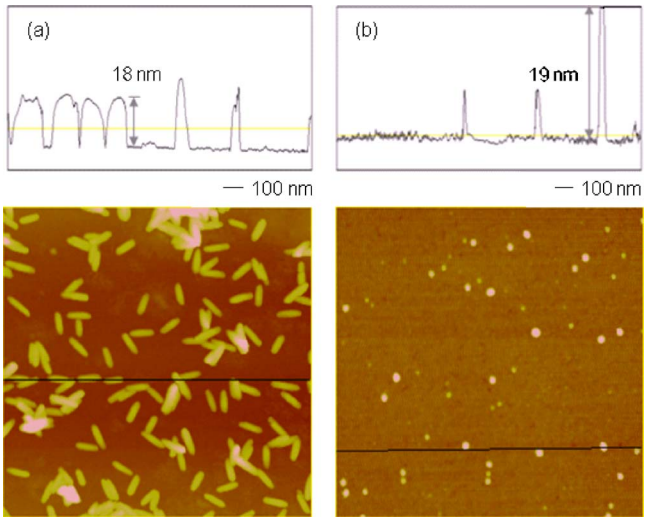

FIG. 3. (Color online) Tapping-mode AFM micrographs of (a) oval-shaped nanorods and (b) spherical Fe nanoparticles. The top panels show the height profiles along the horizontal lines in the respective micrographs.

709.8 eV (with the corresponding shakeup feature at 716.0 eV) became more evident. Further sputtering caused both of these features to reduce in intensity [as shown also in the inset of Fig. 2(c)]. The small shift in the O 1*s* peak for SiO_2 to 531.6 eV was caused by sputtering, while the weak O 1*s* peak for FeO at 530.3 eV was overwhelmed by the predominant O 1*s* peak for SiO_2 [Fig. 2(b)].

Oval-shaped nanorod and spherical nanoparticles of Fe were obtained on the Si substrate by electrodeposition at two different concentrations of $FeCl_3$ solution. It is well known that nanoscale FeOOH colloidal particles (without any metallic Fe core inside) can be formed by hydrolysis in an aqueous $FeCl_3$ solution, and these colloidal particles are found to have an oval-shaped nanorod structure.[16] The hydrolysis of $FeCl_3$ depends on several parameters, including the Fe^{3+} concentration, temperature, *p*H, and the age of the solution. The different concentrations of the $FeCl_3$ solution employed in the present work should give rise to different degrees of hydrolysis. At a higher $FeCl_3$ concentration, we therefore expect the formation of more FeOOH colloidal particles. The oval shape of the nanorod nanostructure could therefore be due to codeposition of FeOOH during electrodeposition of the Fe nanoparticles at the higher concentration of $FeCl_3$. On the other hand, a lower concentration of $FeCl_3$ would give rise to a lesser extent of hydrolysis and therefore a lower concentration of FeOOH colloidal particles. The formation of spherical nanoparticles (without any FeOOH detected in the oxide shell) at a low $FeCl_3$ concentration is therefore consistent with this picture. It should be noted that during electrodeposition of both the oval-shaped nanorods and spherical nanoparticles, the current transients were found to increase near-linearly with the square root of the deposition time. The observed dependence is characteristic of instantaneous nucleation and that the nanoparticle deposition follows the island growth mode.

In summary, near-monosized (130 nm × 25 nm diam.) and uniformly distributed oval-shaped nanorod Fe particles have been produced by electrodeposition on a H-terminated Si(100) substrate at a typical $FeCl_3$ concentration of 10 mM. At a lower $FeCl_3$ concentration of 0.1 mM, spherically shaped Fe nanoparticles (6–40 nm) approaching the quantum size limit were obtained. In the AFM micrographs shown in

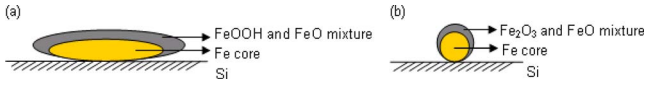

FIG. 4. (Color online) Schematic diagrams of the Fe core-shell nanostructures of (a) oval-shaped nanorods and (b) spherical nanoparticles. It should be noted that the exact shape of the Fe core is not known.

Fig. 3, we illustrate the different topographical features of the oval-shaped nanorods and spherical Fe nanoparticles. These AFM images confirm the morphological features of the Fe nanostructures as shown in the respective SEM images in Figs. 1 and 2. Depth-profiling XPS analysis shows that after removal of a thin layer of surface Fe_3O_4 (likely produced by air oxidation), the nanorods are found to consist of a substantial metallic Fe core (~75%) and a mixed oxide shell of FeOOH and FeO [Fig. 4(a)]. The spherical nanoparticles also consist of an Fe core with a similar shell-to-core thickness ratio as the nanorods but with a different mixture of Fe_2O_3 and FeO in the external shell [Fig. 4(b)]. The remarkably different shapes of these nanoparticles obtained at different $FeCl_3$ concentrations lead us to propose that codeposition of FeOOH (due to hydrolysis in the $FeCl_3$ solution) is responsible for the oval-shaped nanorod structures. Furthermore, as the cores of both types of nanoparticles are metallic Fe, interesting magnetic properties, particularly those of the oval-shaped nanorod nanostructure, are expected.[12] While a fairly narrow size distribution of the oval-shaped nanorods could be achieved by the present electrochemical deposition method, the smaller spherical nanoparticles, with some approaching the quantum size regime, are found to exhibit a considerably broader size distribution. Studies into acquiring further control of the size distribution of these spherical nanoparticles are currently in progress.

This work was supported by the Natural Sciences and Engineering Research Council (NSERC) of Canada.

[1] S. Sun, C. B. Murray, D. Weller, L. Folks, and A. Moser, Science **287**, 1989 (2000).
[2] P. Tartaj, M. P. Morales, S. Veintemillas-Verdaguer, T. González-Carreño, and C. J. Serna, J. Phys. D **36**, R182 (2003).
[3] S. Gangopadhyay, G. C. Hadjipanayis, S. I. Shah, C. M. Sorensen, K. J. Klabunde, V. Papaefthymiou, and A. Kostikas, J. Appl. Phys. **70**, 5888 (1991).
[4] Y. Q. Li, P. Xiong, S. von Molnár, S. Wirth, Y. Ohno, and H. Ohno, Appl. Phys. Lett. **80**, 4644 (2002).
[5] A. D. Kent, T. M. Shaw, S. von Molnár, and D. D. Awschalom, Science **262**, 1249 (1993).
[6] M. A. McCord and D. D. Awschalom, Appl. Phys. Lett. **57**, 2153 (1990).
[7] S. Jain, S. Y. Chan, A. O. Adeyeye, and C. B. Boothroyd, Int. J. Nanosci. **3**, 631 (2004).
[8] H. A. Hosein, D. R. Strongin, M. Allen, and T. Douglas, Langmuir **20**, 10283 (2004).
[9] M. Schlesinger and M. Paunovic, *Modern Electroplating*, 4th ed. (Wiley, New York, 2000), p. 461.
[10] X. J. Zhou, A. J. Harmer, N. F. Heinig, and K. T. Leung, Langmuir **20**, 5109 (2004).
[11] *Handbook of Semiconductor Wafer Cleaning Technology*, edited by W. Kern (Noyes, Park Ridge, NJ, 1993).
[12] L. Y. Zhao and K. T. Leung (unpublished).
[13] J. F. Moulder, W. F. Stickle, P. E. Sobol, and K. D. Bomben, in *Handbook of X-Ray Photoelectron Spectroscopy*, 2nd ed., edited by J. Chastain (Perkin-Elmer, Eden Prairie, MN, 1992).
[14] T. Choudhury, S. O. Saied, J. L. Sullivan, and A. M. Abbot, J. Phys. D **22**, 1185 (1989).
[15] G. C. Allen, M. T. Curtis, A. J. Hooper, and P. M. Tucker, J. Chem. Soc. Dalton Trans. **14**, 1525 (1974).
[16] S. Musić, S. Krehula, S. Popović, and Ž Skoko, Mater. Lett. **57**, 1096 (2003).